C. elegans THSC/TREX-2 deficiency causes replication stress and genome instability

Angelina Zheleva[1], Lola P Camino[1,2], Nuria Fernández-Fernández[1,2], María García-Rubio[1,2], Peter Askjaer[3], Tatiana García-Muse[1,2]* and Andrés Aguilera[1,2]

[1]*Centro Andaluz de Biología Molecular y Medicina Regenerativa-CABIMER, Universidad de Sevilla-Consejo Superior de Investigaciones Científicas-Universidad Pablo de Olavide, 41092 Seville, Spain.* [2]*Departamento de Genética, Facultad de Biología, Universidad de Sevilla, 41012 Seville, Spain.* [3]*Centro Andaluz de Biología del Desarrollo (CABD), Consejo Superior de Investigaciones Científicas-Universidad Pablo de Olavide, 41013 Seville, Spain.*

**Corresponding author.* E-mail: tatiana.muse@cabimer.es

Key words: *C. elegans,* THSC/TREX-2 complex, replication, DNA-RNA hybrids, genome instability

ABSTRACT

Transcription is an essential process of DNA metabolism, yet it makes DNA more susceptible to DNA damage. THSC/TREX-2 is a conserved eukaryotic protein complex with a key role in mRNP biogenesis and maturation that prevents genome instability. One source of such instability is linked to transcription as shown in yeast and human cells, but the underlying mechanism and whether is universal is still unclear. To get further insight in the putative role of THSC/TREX-2 in genome integrity we have used *Caenorhabditis elegans* mutants of the *THP*-1 and *DSS*-1 members of THSC/TREX-2. These mutants show similar defective meiosis, DNA damage accumulation and activation of the DNA damage checkpoint. However, they differ regarding replication defects as determined by dUTP incorporation in the germline. Interestingly, this specific *thp-1* phenotype can be partially rescued by overexpression of RNase H. Furthermore, both mutants show a mild increase in the H3S10P mark previously shown to be linked to DNA-RNA hybrid-mediated genome instability. These data support the view that both THSC/TREX-2 factors prevent

transcription-associated DNA damage derived from DNA-RNA hybrid accumulation by separate means.

INTRODUCTION

Defects in the coupling of transcription with mRNA processing and export results in DNA damage and genome instability (Gaillard *et al*, 2013; Gómez-González and Aguilera, 2019). Understanding the link between mRNA biogenesis and genome instability has benefited strongly from studies of the THO complex, required for transcription elongation, mRNA export and genome integrity (Luna *et al*, 2012). Mutations in THO components give rise to not only transcription defects but also to genetic instability exhibited as hyper-recombination and DNA damage accumulation. These phenotypes are partially explained by the accumulation of R-loops in THO mutants in yeast, worms and human cells. An R loop is a three-stranded structure formed during transcription by hybridization of the nascent RNA with the transcribed DNA strand, displacing the non-transcribed strand as single-strand DNA (ssDNA) (Huertas and Aguilera, 2003; Castellano-Pozo *et al*, 2012a; Domínguez-Sánchez *et al*, 2011b). Although R-loops form naturally as key intermediates in specific cellular processes, such as *E. coli* plasmid replication, mitochondrial DNA replication or immunoglobulin (Ig) class switching (Aguilera and Garcia-Muse, 2012), unscheduled R-loops are an important player in genome instability. Increasing evidence from yeast to mammals reveals that mRNA processing defects cause genetic instability in an R-loop-dependent manner, since the removal of these DNA-RNA hybrids partially suppresses the genetic instability phenotypes (Crossley *et al*, 2019). Previously, we have used the simple metazoan *Caenorhabditis elegans* to uncover a new role for the THO complex in development and meiosis and demonstrated that the defects in meiosis were partially due to replication impairment derived from R-loop accumulation in THO mutants (Castellano-Pozo *et al*, 2012b, 2012a). Moreover, we reported a link between R-loops and the H3S10P, a marker of chromatin condensation, and H3K9me2, a marker of heterochromatin, which suggest a role for RNA in chromatin compaction or condensation (Castellano-Pozo *et al*, 2013; Garcia-Pichardo *et al*, 2017). Interestingly, the H3K9me2 modification has also been linked to R loops occurring at transcription termination regions of some genes as well as in some rare fragile sites (Skourti-Stathaki *et al*, 2014; Groh *et al*, 2014). This connection between chromatin structure and R loop accumulation adds new elements to understand how R loops modulate genome dynamics.

The THSC/TREX-2 complex is conserved from yeast to humans and is involved in mRNP biogenesis (Garcia-Oliver *et al*, 2012; Rondón *et al*, 2010). It interacts with the nuclear pore complex (NPC) and is constituted by the stable association of the multi-domain protein Sac3/GANP with the Thp1/PCID2, Sus1/ENY2, Cdc31/CEN2 and Sem1/DSS1 subunits (Fischer *et al*, 2002; Gallardo *et al*, 2003; Lei *et al*, 2003), among which Cdc31 and Dss1 have also been characterized as a centrin and a 19S proteosome subunit, respectively (Faza *et al*, 2009; Fischer *et al*, 2004; Wilmes *et al*, 2008). In addition to these functions, the mammalian proteins PCID2 and DSS1 have been linked to BRCA2 (breast cancer susceptibility gene 2 product), a component of the homologous recombination machinery (Bhatia *et al*, 2014; Marston *et al*, 1999; Yang *et al*, 2002). Similarly to THO, it is believed that the genetic instability and transcriptional defects observed in yeast THSC/TREX-2 mutants (Gallardo *et al*, 2003) are due to R-loop accumulation as co-transcriptional cleavage of the nascent RNA reduced both defects to some extent (González-Aguilera *et al*, 2008). However, our laboratory has shown that depletion of PCID2, despite increasing genomic instability, does not lead to detectable accumulation of R-loops (Bhatia *et al*, 2014). To shed light into this conundrum we have used the nematode *C. elegans* to characterize two putative members of the *C. elegans* THSC/TREX-2 complex. We have observed that lack of the CeTHP-1 component of THSC/TREX-2 leads to sterility, DNA damage accumulation and replication defects at the germline. Importantly, microinjection of RNase H partially restores the Cy3-dUTP incorporation in the nematode germline consistent with R-loops interfering with replication progression. Interestingly, there is only a mild increase in the H3S10P chromatin mark in the THSC/TREX-2 mutants analyzed, strengthening the idea that R-loops interfere with replication in different ways. Our data provides evidence that THSC/TREX-2 contributes to the maintenance of genome integrity in part by preventing R loop accumulation. Hence this study highlights that cells have developed alternative ways to avert DNA-RNA hybrids and minimize their incidence as a source of DNA damage and genome instability.

RESULTS

C.elegans THSC/TREX-2 complex is essential for fertility

To analyze the role of THSC/TREX-2 in *C. elegans*, first we performed a search of THSC/TREX-2 orthologs based on the sequence comparison (Garcia-Oliver *et al*, 2012). The putative components of the *C. elegans* THSC/TREX-2 complex are summarized in Table S1. In yeast, Thp1, Sac3, Sus1 and Cdc13 are stable associated subunits of the THSC/TREX-2 complex (Gallardo et al. 2003) while Sem1 shown to also be an integrating

component of TREX-2 (Wilmes *et al.,* 2008; Faza *et al*., 2009), is a subunit of the 19S proteasome that interact with other factors, as BRCA2 in mammals (Marston *et al*, 1999; Yang *et al*, 2002). To investigate the similar or different effects of these two THSC/TREX-2 complex members we decided to work with these two candidates for further analysis: the C27F2.10 gene (from now on *thp-1*) homolog to yeast *THP1* and human PCID2, and the *dss-1* homolog to yeast *SEM1* and human DSS1. The CeTHP-1 protein displays a 45% and 27% amino-acid identity with human PCID2 and yeast Thp1, respectively (Fischer *et al*, 2002; Jani *et al*, 2012) (Table S1). Similarly to human PCID2 (Umlauf *et al*, 2013), we show here that CeTHP-1 is a nuclear protein and accumulates at the nuclear periphery, possibly at nuclear pore complexes (Fig. S1A,B). CeDSS-1 displays a 49% and 40% amino-acid identity with human DSS1 and yeast Sem1, respectively (Pispa *et al*, 2008) (Table 1).

We investigated the two THSC/TREX-2 *C. elegans* orthologs by characterizing two deletion mutants, *thp-1(tm3507)* and *dss-1(tm370)*, which are predicted to encode non-functional truncated proteins. The *thp-1* gene spans 1.9 kb, including 9 exons, and is predicted to encode an mRNA that produces a 413 amino-acid protein (Fig. S1C). The *thp-1(tm3507)* allele carries a deletion of 255 bp that can be detected by single worm PCR (Fig. S1D), and is predicted to encode a non-functional truncated protein of 64 amino acids corresponding to the first three exons and part of the fourth one. The *dss-1* gene was previously characterized as crucial for embryogenesis, larval growth and oogenesis (Pispa *et al*, 2008). Lethality assays revealed that the *thp-1(tm3507)* allele conferred complete sterility, since the mutant homozygous strain laid no eggs (Table 1), while N2(wt) and heterozygous *thp-1(tm3507)* mutants show the expected lethal percentage 0.05% and 62.86% respectively. The lethality observed in the heterozygous mutant is due to the nature of the balancer system used (Edgley *et al*, 2006). The data demonstrated that lack of the THSC/TREX-2 component THP-1 leads to sterility similarly to that previously described for the *dss-1* mutant (Pispa *et al*, 2008). Therefore, the *C. elegans thp-1* is an essential gene, as is *dss-1*. Yet, homozygous mutants produced by self-fertilization of heterozygous hermaphrodite parents are rescued beyond L4 stage by maternal contribution of *thp-1* and *dss-1* mRNA, allowing the analysis of mutants defective in either gene within adult tissues.

To determine whether the sterility phenotype was caused by a defect during meiosis, we analyzed *thp-1(tm3507)* and *dss-1(tm370)* germlines. Each germline is spatially polarized in a distal to proximal manner with respect to mitotic proliferation and progression through meiotic prophase I. In the distal region nuclei proliferate by mitotic divisions acting as stem cells until they reach the transition zone where meiosis starts (Garcia-Muse and Boulton, 2007). 4,6-Diamidino-2-phenylindole (DAPI) staining of *thp-1(tm3507)* and *dss-1(tm370)* germlines showed a mitotic region slightly reduced with respect to the N2(wt) regarding the number (Fig. 1).

At the proximal region of the germline, wild type oocytes always have nuclei with six discernible DAPI-stained bivalent chromosomes, indicative of successful meiosis I. In *C. elegans* any variation on this number is considered an aneuploidy due to defective meiosis. Indeed, as can be seen in Fig. 2A, N2 (wild type) oocytes show 6 bivalents (average 6±0.0, n=51), whereas in the case of the *thp-1* mutant oocytes with six normally condensing chromosomes as well as oocytes with more than six bivalents (average 7,6±1,67, n=45) were observed. This is an observation shared with the *dss-1* mutant, where oocytes also show a deviation from the expected number of six condensed chromosomes (average 7,32±1,59, n=65), that it has been show to increase with the age of the animal (Fig. 2A, (Pispa *et al*, 2008)). This implies that both *thp-1* and *dss-1* mutants have abnormal diakinesis. In 24h post-L4 animals we were not able to see any difference in the number of oocytes respect to the N2(wt) that shows 4-5, however older *thp-1* animals would show alterations in the organization of the proximal region, being difficult to differentiate diplotene and diakinesis (Fig. 2B).

DNA damage and checkpoint activation in *thp-1* and *dss-1* mutants

Next, we analyzed whether the diakinesis defect could be a consequence of early meiotic defects. One essential feature of successful meiosis is the meiotic recombination, which is required for the generation of genetic variation and for proper chromosome segregation. Meiotic recombination is initiated by SPO-11-dependent DSB formation (Dernburg *et al*, 1998), and requires RAD-51, a member of the RecA-strand exchange protein family, to catalyze the invasion of DNA single-strand overhangs into a recipient double-strand DNA to initiate formation of D loops and the later steps of meiotic recombination (West, 2003). First, to examine DSBs during meiosis in *thp-1* and *dss-1* mutants we analyzed RAD-51 foci (Alpi *et al*, 2003). In N2(wt) worms, the levels of RAD-51 foci increased upon entrance to the transition zone (zone 2), peaked at mid-pachytene (zone 4) and disappeared by the end of pachytene (zone 5; Fig. 3). Upon entrance into meiosis (zone 3), *thp-1* and *dss-1* mutants accumulated RAD-51 foci earlier than N2(wt) worms (Fig. 3; Fig. S2), suggesting that the DSBs observed could originate from problems during mitotic replication or pre-meiotic replication at the entrance of the transition zone. Also, in these mutants we observed that RAD-51 foci remained until the end of the germline implying that DSBs do not repair with the efficiency of N2(wt) animals (Fig. 3; Fig. S2). With the aim to check if the increase in DSB observed in *thp-1* was due to a defect in their repair we performed a DSB repair analysis. 24h post-L4 animals were treated with 75Gy (which generates mainly DSBs), leaved for 36-48 hours and then RAD-51 foci accumulation was analyzed. At mitotic and transition zone regions N2(wt) animals the levels of RAD-51 were similar to the non-treated control worms while the *thp-1* irradiated shows a decrease in the nuclei without RAD-51 foci with respect to

the non-treated (Fig. S3). This is can also be observed in the meiotic regions, although at 36 hours the N2(wt) is not completely recovered the *thp-1* mutant shows a more dramatic accumulation of DSB when comparing both irradiated and not treated (Fig. S3). These results suggest that in *thp-1* DSB repair is compromised.

To determine if the increase in DSBs in *thp*-1 and *dss*-1 mutants was a readout of DNA damage caused by replication problems we performed immunofluorescence using antibodies against the single-strand binding protein RPA-1, which is involved in replication and recombination, and against the DNA damage checkpoint protein ATL-1, which is recruited to sites of DNA damage where it activates the DNA damage checkpoint (Garcia-Muse and Boulton, 2005, Stergiou *et al*. 2011). Unlike N2(wt) worms, *thp-1* and *dss-1* mutants exhibited regions of ssDNA as indicated by the presence of RPA-1 and ATL-1 foci in mitotic and meiotic nuclei (Fig. 4; Fig. S5). This is consistent with the interpretation that DNA damage is occurring (throughout the germline) in *thp-1* and *dss-1* mutants, and subsequently activating the DNA damage checkpoint. This phenotype is reminiscent of that observed in *thoc-2* mutants (Castellano-Pozo *et al*, 2012a) and mutants with defects during S-phase such as *atl-1* and *clk-2*, in which endogenous DNA breaks arise from replication defects (Ahmed *et al*, 2001; Garcia-Muse and Boulton, 2005).

DNA replication impairment in *thp-1* mutants

To examine if the absence of THP-1 and DSS-1 proteins of the THSC/TREX-2 complex hinders replication we assessed incorporation of deoxyribonucleotides into germlines DNA after microinjection of Cy3-dUTP into young adults hermaphrodite germlines (Castellano-Pozo *et al*, 2012a; Jaramillo-Lambert *et al*, 2007). In N2(wt) and *dss-1* worms all germlines showed Cy3-dUTP incorporation in all mitotic nuclei (Fig. 5; Fig. S5). However, the number of nuclei that incorporated Cy3-dUTP was significantly reduced in *thp-1* mutants (Fig. 5). This result demonstrates that mitotic replication is impaired in *thp-1* mutants but not in *dss-1*.

In yeast and *C. elegans,* other mRNA biogenesis mutants such as mutants from the THO complex also show replication defects. These defects have been linked to R-loop accumulation (Castellano-Pozo *et al*, 2012a; Huertas and Aguilera, 2003; Wellinger *et al*., 2006). To address directly if this was also the case in *thp-1* mutant, we co-microinjected *Escherichia coli* RNase H1, which specifically digest the RNA moiety of DNA-RNA hybrids, into the worms in our *in vivo* replication assay (Castellano-Pozo *et al*, 2012a). Co-microinjection of RNase H1 did not affect incorporation of Cy3-dUTP in N2(wt) worms, whereas in *thp-1* mutants caused a clear increase in Cy3-dUTP labeled nuclei (Fig. 5). Although incomplete, a partial recovery of mitosis proficiency was possible upon RNase H1 microinjection. This result suggests that R-loops can form in *thp-1 C. elegans* mutant and

could be responsible for the mitotic replication impairment that leads to the DNA damage observed.

It is not yet well understood the mechanism and factors responsible for genome instability mediated by R-loops. We previously found that R-loops are linked to H3S10 phosphorylation, a mark of chromatin condensation, which led us to propose a model in which R-loops trigger the formation of condensed chromatin patches that would interfere with replication and/or transcription (Castellano-Pozo *et al*, 2012a). This conclusion was reinforced by the identification of yeast histone mutants unable to phosphorylate histone H3S10P (due to the lack of the residue or its mutation into alanine), which were able to accumulate high levels of R loops although without compromising genome integrity (Garcia-Pichardo *et al*, 2017). To determine if R-loop-mediated chromatin modifications could explain the genome instability of THSC/TREX-2 *C. elegans* mutants, we performed immunostaining against H3S10P. Normally a N2(wt) germline shows 1-2 mitotic nuclei with H3S10P correlating with chromosome condensation during mitosis and at the compacted bivalents of the diakinesis region (Fig. 6; Fig.S6). We observed a slight increase of nuclei with H3S10P signal in both mutants, which was clearer in *thp-1* (Fig. 6). In this mutant some nuclei with H3S10P signal were observed beyond the germline mitotic region, reaching the transition zone and early pachytene regions (Fig. 6; Fig.S6). In addition, we observed H3S10P at later meiosis stages, in N2(wt) the compacted six bivalents show a bright signal like the *thp-1* and *dss-1* mutants. We noticed that 36h post-L4 worms, when diakinesis is more disorganized in the *thp-1* mutant, H3S10P signal could be seeing at the late pachytene region (Fig. 2B; Fig. S6B). Thus, at least part of the observed replication impairment could be due to chromatin compaction triggered by R-loops as it has been shown in yeast and mammals (Castellano-Pozo et al, 2013).

DISCUSSION

Failures of DNA metabolism processes such as DNA replication and repair are a major source of DNA damage accumulation in cells (Aguilera and Garcia-Muse, 2013). Importantly, it has been shown that DNA damage occurs at higher levels at regions with high transcriptional activity. Indeed, the loss of several RNA processing factors is associated with genome instability which is explained, in part, by the formation of co-transcriptional DNA-RNA hybrids (Aguilera and Garcia-Muse, 2012; Garcia-Muse and Aguilera, 2019). To further understand this process in pluricellular organisms we have analyzed mitosis and meiosis in *C. elegans* depleted of the THSC/TREX-2 mRNP biogenesis complex. Analysis of deletion mutants of two components of THSC/TREX-2, *thp-1(tm3507)* and *dss-1(tm370),* revealed

that this complex is required for fertility since the mutants do not lay eggs. The absence of eggs is not due to compromised gonad development since a two-arm gonad with developing germ cells was present in all mutant worms examined. Germline analysis of both TREX-2 mutants reveled defects in diakinesis since oocyctes with an abnormal number of bivalents were observed. Nevertheless, the eggless phenotype cannot be explained neither by the diakinesis defects observed in the *thp*-1 and *dss*-1 mutants since other mutants with defective diakinesis do form and lay eggs, and the lethality is observed at the embryonic stage. This is the case of mutants of *brc*-2, the *C. elegans* homologue of DNA repair gene *BRCA-2* (Martin *et al*, 2005; Pispa *et al*, 2008). BRCA2 interacts with DSS1 (Marston *et al*, 1999; Yang *et al*, 2002) and loss of either BRCA2 or DSS1 results in defects in homologous recombination (West, 2003). However, in *brc*-2 mutant oocytes chromosomes aggregate instead of condensing normally and produce eggs unlike *thp*-1 and *dss-1* mutants. One proposed reason for *dss-1* oogenesis defects is an aberrant regulation of the degradation of some essential protein required for oogenesis, on the basis that DSS1 is also a component of the proteasome (Krogan *et al*, 2004). Another possibility it could relay in its relationship with BRCA2 (Bhatia et al., 2014). Yet, the fact that the mutant of the THSC/TREX-2 mRNA biogenesis complex, *thp-1*, shares the same eggless phenotype suggest a second possibility of an indirect effect caused by a defect in the mRNA biogenesis of specific meiotic genes. Nevertheless, our observations open a third possibility, which would need to be further investigated, in which R-loop accumulation could also contribute to this eggless phenotype, as described for mutants of the THO complex (Castellano-Pozo *et al*, 2012).

C. elegans thp-1 and *dss-1* mutants show a clear increase in genome instability as determined by accumulation of RPA-1 and RAD-51 foci and checkpoint activation. DNA damage accumulation, if not properly repaired, leads to genetic alterations such as mutations, gross chromosomal rearrangements, hyper-recombination and loss of heterozygosis, all highlights of genome instability. Genome instability may result from failures at different DNA processes, yet, failures in DNA replication is one of the most common causes (Aguilera and Garcia-Muse, 2013). Replication impairment leads to ssDNA gaps and DSB accumulation. Most likely this DNA damage accumulation is the source of genomic instability observed in *thp-1*. Indeed, loss of TREX-2 complex in the worm leads to impaired replication as observed with our *in vivo* replication assay. One cause of this defect could be the replication-transcription conflicts favored by the presence of DNA-RNA hybrids. In agreement with this, replication impairment can be partially suppressed by the addition of RNase H that removes DNA-RNA hybrids. This observation supports that the defective replication due to the loss of a core component of the THSC/TREX-2 is in part caused by DNA:RNA hybrids, as it is also the case for the absence of a functional THO complex in all organisms analyzed (Castellano-Pozo *et al*, 2012a; Huertas and Aguilera, 2003;

Domínguez-Sánchez *et al*, 2011a). In contrast, loss of *dss-1* does not hamper replication, suggesting that the genomic instability observed in this mutant is more likely to be related with BRCA2 (Pispa *et al.*, 2008; Bhatia *et al*., 2014). In addition to cause the generation of DSBs, R-loops have recently been shown to accumulate at DSBs, especially those induced in transcriptionally active loci. However, is still unclear the significance of this, since data supporting both that R-loops actively participate or that interfere in DSB repair has been shown (AguileraandGomez-Gonzalez, 2017; Marnef and Legube, 2020). We have observed that *thp-1* mutants show a delay in repair, which is in harmony with a detrimental effect of R loops in DSB repair. In other hand, it has been shown that spontaneous R loops must be removed to avoid genomic instability and that repair factors such as BRCA2 play a role in this (Bhatia et al., 2014; D'Alessandro et al., 2018), and, as we mentioned above, this could be behind the differences observed between the *thp-1* and *dss-1* mutants. Therefore, our results show how two components of the *C. elegans* THSC/TREX-2 impact differently in genome stability.

Co-transcriptional assembly of proteins on the nascent RNA is a conserved strategy to prevent formation of DNA-RNA hybrids from bacteria to eukaryotes (Garcia-Muse and Aguilera, 2019; Aguilera and Garcia-Muse, 2012). In bacteria translation occurs co-transcriptionally likely preventing the invasion of the RNA molecule during its synthesis (Gowrishankar and Harinarayanan, 2004). In yeast and metazoans many RNA processing and splicing factors assemble within the RNA strand, therefore preventing the accumulation of DNA-RNA hybrids (Huertas and Aguilera, 2003; Li and Manley, 2005; Domínguez-Sánchez *et al*, 2011a). The number and complexity of RNA processing, splicing and export factors is increased in metazoans respect to yeast. This could be behind the fact that although depletion of yeast TREX-2 complex leads to genome instability partially dependent on DNA-RNA hybrids (González-Aguilera *et al*, 2008), this is not that evident for vertebrate PCID2 ortholog of *THP-1*. Although PCID2 prevents genome instability, its depletion does not lead to a detectable accumulation of DNA:RNA hybrids (Bhatia *et al*, 2014), albeit we cannot discard it is a matter of methodology limitations or could be evident for other components of TREX-2 *such as* GANP, yet to determined. Our results in the nematode correlate with the ones obtained previously in yeast, in which THSC/TREX-2 complex helps prevent genome instability derived from DNA-RNA hybrid accumulation, opening the possibility is that these THSC/TREX-2 function might have evolved after the divergence of nematodes from the main metazoan lineage.

How the presence of DNA-RNA hybrids causes the replication-transcription conflicts is yet not completely resolved. A higher impact of hybrids in convergent versus co-directional collisions has been described also (Hamperl *et al*, 2017; Garcia-Rubio *et al*, 2018; Lang *et al*, 2017). We have described that DNA-RNA hybrids can alter chromatin increasing the

presence of the condensation mark H3S10P and heterochromatin H3K9me^2 in nematode THO mutants (Castellano-Pozo *et al*, 2013). Similar observations have been obtained in other DNA-RNA hybrid-accumulating mutants from yeast to metazoans (Colak *et al*, 2014; Loomis *et al*, 2014; Skourti-Stathaki *et al*, 2014). The relevance of histone marks has been further confirmed by the identification of yeast histone mutations that facilitate DNA-RNA hybrid but do not cause instability in agreement with the fact that they are not able to accumulate H3S10P (Garcia-Pichardo *et al*, 2017). Importantly, such histone mutations suppress the genome instability phenotype of *hpr1* and *sen1* mutants because they prevent H3S10 phosphorylation (Garcia-Pichardo *et al*, 2017). Unlike THO-complex mutants the loss of THSC/TREX-2 in *C. elegans* causes a mild increase of the condensation mark H3S10P, whereas replication is impaired at similar levels in mutants of both complexes. This suggests that a putative premature condensation may not be the only way by which DNA-RNA hybrids can generate transcription-associated genome instability. In this sense, we have recently shown that hybrid stabilization by overexpression of the Yra1 RNA-binding protein also causes R loop-mediated genome instability (Gavaldá *et al*, 2016; Garcia-Rubio *et al*, 2018).

Lastly, there are important differences between the THO and the THSC/TREX-2 complexes, and likely the mechanism by which R loop accumulation leads to genetic instability. During mRNA biogenesis the two complexes act at different steps. The THO complex is recruited to chromatin and is required early during transcription elongation and mRNA export. Additional proteins would be recruited to the nascent mRNP via THO to later on facilitate the recruitment of THSC/TREX-2 to bind the mRNP to the nuclear pore complex (NPC). Importantly, it has been shown that physical proximity of transcribed chromatin to NPCs restrains the formation of pathological R loops during transcription (Garcia-Benitez *et al*, 2017). This observation agrees with the gene-gating hypothesis, which proposes that localization of transcribed DNA at the NPC facilitates the formation of an export-competent mRNP (Blobel, 1985). While this mechanism is well characterized in yeast it is less defined in mammalian cells, for which further studies would be required for cells depleted of different THSC/TREX-2- factors. In this regard *C. elegans* has been shown to have developmental and stress-induced gene gating (Rohner *et al*, 2013) and we provide evidence that THSC/TREX-2 accumulates at the nuclear periphery. This grants the hypothesis that R loop-dependent phenotypes observed in the THSC/TREX-2 mutants could be originated by defects in the association with the NPC in line with data provided for Mlp1,2 yeast mutants.

MATERIALS AND METHODS

Strains and maintenance

Standard methods were used for the maintenance and manipulation of *C. elegans* strains (Brenner, 1974). The wild type Bristol N2 and JK2739 nematode strains were provided by the *Caenorhabditis* Genetics Center, which is funded by the NIH National Center for Research Resources. *dss-1(tm370)* was kindly provided by Dr. Jäntti (Pispa *et al*, 2008) and *thp-1(tm3507)* was generated and kindly provided by Dr. Mitani. *C. elegans thp-1(tm3507)* deletion was backcrossed six times with wild type Bristol N2 and then balanced with JK2739. The presence of *thp-1(tm13507)* and *dss-1(tm350*) deletion alleles was determined by nested PCR (primers are listed in Table S2). The RPA-1::YFP(ops263) is described in Stergiou et al, 2011.

Embryonic lethality was scored by comparing the number of eggs that hatch to produce viable progeny versus the total number of eggs laid. Briefly L4 hermaphrodites grown at 20°C were individually plated. The animals were transferred to new plates once every 24 hours until the egg laying stopped. Every day eggs laid and hatched larvae were counted. The total number of single hermaphrodites for each stain is indicated in Table 1. Homozygous hermaphrodites used were *thp-1(tm3507)* mutants derived from *thp-1(tm3507)* heterozygous parents.

For DNA repair analysis after irradiation, 24h. post-L4 animals were exposed to 75 Gy of γ-ray from BioBeam8000. After 36-48h. post-irradiation worms were processed for gonad analysis by immunofluorescence. As control non-Irradiated plates were maintained in parallel.

To express GFP::THP-1, we inserted a full-length *thp-1* PCR product amplified from N2 genomic DNA into plasmid pBN16, which contains a heat-inducible *hsp-16.41* promoter and the 3'UTR of *unc-54* (Ródenas *et al*, 2012). The resulting plasmid, designated pBN467, was used for Mos-mediated single copy integration into *ttTi5605* on chrII of EG4322 (Frøkjær-Jensen *et al*, 2008) to generate strain BN967, which next was crossed to BN903 that has mKate2 inserted into the 5'-end of the *mel-28* coding sequence, resulting in strain BN974. Tagging of MEL-28, which localises to nuclear pore complexes, with mKate2 was done similarly to the protocol for insertion of GFP into the *mel-28* locus (Gomez-Saldivar *et al*., 2016).

Immunostaining

Immunofluorescences for Figures 2 and 5 were performed as described (Martin *et al*, 2005). One day post-L4 adult gonads were dissected in PBS with levimasole on polylisine slides, fixed for 20 m. in 4% paraformaldehyde and replaced for 10 min. in TBSBTx (TBSB + 0.4% TX100). The slides were washed twice for 10 min. and once for 30 min. with TBSB (TBS + 0.5% BSA). They were incubated overnight at 4ºC with the 1ry antibodies (Table S3). Next day gonads were washed 3 times in TBSB, each for 30 minutes at RT, and incubated for 2 hours with the secondary antibody in TBSB (Table S3). Gonads were washed three times for 30 minutes in TBSB and mounted with 10 µl Vectashield (with 1 µg/ml DAPI) per sample for further analysis.

Immunofluorescences for Figures S3, S5 were performed as described (Castellano-Pozo et al., 2020), with slight modifications. One day post-L4 adult gonads (but for Figure S3, in which 72h post-L4 gonad were analyzed) were dissected in TBSTw (TBS Tween20 at 1%) on polylisine slides, fixed for 5 min. in 1% paraformaldehyde, freeze in liquid nitrogen and permeabilysed 10 min. MeOH -20Cº. The slides were washed with TBSTw 3 times for 5 min. and blocked for 30 min. with TBSTwB (TBSTw + 0.7% BSA). They were incubated overnight at 4ºC with the 1ry antibodies (Table S3). Next day gonads were washed 3 times in TBSTw, each for 10 min., and incubated for 2 hours with the secondary antibody in TBSB (Table S3). Gonads were washed once in TBSTw+DAPI (1 µg/ml) for 10 min. and then washed 4 times for 10 min. in TBSTw and mounted with 10 µl Vectashield per sample for further analysis.

In situ detection of germline DNA synthesis

Direct incorporation of Cy3-dUTP (Amersham Bioscences) into germline nuclei was performed as described (Castellano-Pozo *et al*, 2012a). The injection mix consisted of 50 µM Cy3-dUTP (Amersham Bioscences, Piscataway, NJ) in PBS, pH 7.2. After ~2.5 hours of exposure to the Cy3-dUTP, gonads were dissected, fixed and DAPI-stained. The total number of cells that incorporated Cy3-dUTP was determined for each dissected germline.

Fluorescence microscopy

Images from figures 1A, 2A, 3A, 4 and 5 were acquired with a Leica DM6000B inverted microscope with 40X HCXPL-APO/1.25 OIL or 63X HCXPL-APO/1.40 OIL lens, and images captured using Leica LAS-AF computer software. Regions of interest were projected into one dimension and with Adobe Photoshop CS4 software. Images from al other figures were acquired with a Leica DM6000 inverted microscope with 100X HCXPL-APO/1.40 OIL lens, and images captured using Leica LAS-AF computer software. Regions of interest were projected into one dimension and with Adobe Photoshop CS4 software.

Quantification of Figure 2 was performed counting 10 nuclei of each region from animals along independent experiments (the n is indicated in figure legend). Quantification of Figure 3C and S4 was as in Castellano-Pozo et al. 2020. In brief, all nuclei from animals were conted. Data shows the % of nuclei of the different categories based in the number of foci/nuclei.

Confocal images of GFP::THP-1 and mKate2::MEL-28 were acquired on a Nikon A1R microscope equipped with a Plan Apo VC 60x/1.4 objective (Nikon, Tokyo, Japan) using a pinhole of 1.2 airy unit. Nematodes were grown at 25°C to achieve mild induction of GFP::THP-1 expression. Quantification of fluorescence signal was performed with Fiji, drawing a line 5 pixels wide and 5 µm long from the nuclear center outwards. Background values were obtained from nematodes without expression of fluorescent proteins.

Statistical Analysis

Statistical significance was determined with a Student's t test or ANOVA using PRISM software (Graphpad Software Inc.).

ACKNOWLEDGMENTS

We thank Shohei Mitani at the National Bioresource Project and Dr. Jäntti for kindly providing *thp-1(tm3507)* and *dss-1(tm370)*, some strains were provided by the CGC, which is funded by NIH Office of Research Infrastructure Programs (P40 OD010440), A. Gartner for reagents, and C. Ayuso and U. Galindo for technical assistance. This work was supported by grants from Spanish Ministry of Economy and Competitiveness (BFU2016-

75058-P), European Research Council (ERC) Advanced Investigator Grant (ERC2014 AdG669898 TARLOOP) and the European Union (FEDER).

REFERENCES

Aguilera A and Garcia-Muse T (2012) R loops: from transcription byproducts to threats to genome stability. *Mol. Cell* **46:** 115–124

Aguilera A and Garcia-Muse T (2013) Causes of genome instability. *Annu. Rev. Genet.* **47:** 1–32

Aguilera A, Gómez-González B (2017) DNA-RNA hybrids: the risks of DNA breakage during transcription. *Nat Struct Mol Biol.* **24**: 439-443.

Ahmed S, Alpi A, Hengartner MO and Gartner A (2001) C. elegans RAD-5/CLK-2 defines a new DNA damage checkpoint protein. *Curr. Biol.* **11:** 1934–1944

Alpi A, Pasierbek P, Gartner A and Loidl J (2003) Genetic and cytological characterization of the recombination protein RAD-51 in Caenorhabditis elegans. *Chromosoma* **112:** 6–16

Bhatia V, Barroso SI, Garcia-Rubio ML, Tumini E, Herrera-Moyano E and Aguilera A (2014) BRCA2 prevents R-loop accumulation and associates with TREX-2 mRNA export factor PCID2. *Nature* **511:** 362–365

Blobel G (1985) Gene gating: a hypothesis. *PNAS* **82:** 8527–8529

Brenner S (1974) The genetics of Caenorhabditis elegans. *Genetics* **77:** 71–94

Castellano-Pozo M, Garcia-Muse T and Aguilera A (2012a) R-loops cause replication impairment and genome instability during meiosis. *EMBO Rep.* **13:** 923–929

Castellano-Pozo M, Garcia-Muse T and Aguilera A (2012b) The Caenorhabditis elegans THO Complex Is Required for the Mitotic Cell Cycle and Development. *PLoS One* **7:** e52447

Castellano-Pozo M, Pacheco S, Sioutas G, Jaso-Tamame AL, Dore MH, Karimi MM, Martinez-Perez E (2020) Surveillance of cohesin-supported chromosome structure controls meiotic progression. *Nat Commun.* **11**: 4345.

Castellano-Pozo M, Santos-Pereira JM, Rondón AG, Barroso S, Andújar E, Pérez-Alegre M, Garcia-Muse T and Aguilera A (2013) R Loops Are Linked to Histone H3 S10 Phosphorylation and Chromatin Condensation. *Mol. Cell* **52:** 583–590

Colak D, Zaninovic N, Cohen MS, Rosenwaks Z, Yang W-Y, Gerhardt J, Disney MD and Jaffrey SR (2014) Promoter-bound trinucleotide repeat mRNA drives epigenetic silencing in fragile X syndrome. *Science* **343:** 1002–1005

Crossley MP, Bocek M and Cimprich KA (2019) R-Loops as Cellular Regulators and Genomic Threats. *Mol. Cell* **73:** 398–411

D'Alessandro G, Whelan DR, Howard SM, Vitelli V, Renaudin X, Adamowicz M, Iannelli F, Jones-Weinert CW, Lee M, Matti V et al. (2018) BRCA2 controls DNA:RNA hybrid level at DSBs by mediating RNase H2 recruitment. *Nat Commun.* ***9***: 5376.

Dernburg AF, McDonald K, Moulder G, Barstead R, Dresser M and Villeneuve AM (1998) Meiotic recombination in C. elegans initiates by a conserved mechanism and is dispensable for homologous chromosome synapsis. *Cell* **94:** 387–398

Domínguez-Sánchez MS, Barroso S, Gómez-González B, Luna R and Aguilera A (2011a) Genome instability and transcription elongation impairment in human cells depleted of THO/TREX. *PLoS Genet.* **7:** e1002386

Domínguez-Sánchez MS, Sáez C, Japón MA, Aguilera A and Luna R (2011b) Differential expression of THOC1 and ALY mRNP biogenesis/export factors in human cancers. *BMC Cancer* **11:** 77

Edgley ML, Baillie DL, Riddle DL and Rose AM (2006) Genetic balancers. In *WormBook***:** 1–32 (WormBook, ed.) The C. elegans Research Community, WormBook.

Faza MB, Kemmler S, Jimeno S, González-Aguilera C, Aguilera A, Hurt E and Panse VG (2009) Sem1 is a functional component of the nuclear pore complex-associated messenger RNA export machinery. *J. Cell Biol.* **184:** 833–846

Fischer T, Rodriguez-Navarro S, Pereira G, Rácz A, Schiebel E and Hurt E (2004) Yeast centrin Cdc31 is linked to the nuclear mRNA export machinery. *Nat. Cell Biol.* **6:** 840–848

Fischer T, Strasser K, Racz A, Rodriguez-Navarro S, Oppizzi M, Ihrig P, Lechner J and Hurt E (2002) The mRNA export machinery requires the novel Sac3p-Thp1p complex to dock at the nucleoplasmic entrance of the nuclear pores. *EMBO J.* **21:** 5843–5852

Frøkjær-Jensen C, Davis MW, Hopkins CE, Newman BJ, Thummel JM, Olesen S-P, Grunnet M and Jorgensen EM (2008) Single-copy insertion of transgenes in Caenorhabditis elegans. *Nat. Genet.* **40:** 1375–1383

Gaillard H, Herrera-Moyano E and Aguilera A (2013) Transcription-Associated Genome Instability. *Chem. Rev.* **113**: 8638-8661

Gallardo M, Luna R, Erdjument-Bromage H, Tempst P and Aguilera A (2003) Nab2p and the Thp1p-Sac3p complex functionally interact at the interface between transcription and mRNA metabolism. *J. Biol. Chem.* **278:** 24225–24232

Garcia-Benitez F, Gaillard H and Aguilera A (2017) Physical proximity of chromatin to nuclear pores prevents harmful R loop accumulation contributing to maintain genome stability. *PNAS* **114:** 10942–10947

Garcia-Muse T and Aguilera A (2019) R Loops : From Physiological to Pathological Roles. *Cell* **179**: 604–618

Garcia-Muse T and Boulton SJ (2005) Distinct modes of ATR activation after replication stress and DNA double-strand breaks in Caenorhabditis elegans. *EMBO J.* **24:** 4345–4355

Garcia-Muse T and Boulton SJ (2007) Meiotic recombination in Caenorhabditis elegans. *Chromosome Res.* **15:** 607–621

Garcia-Oliver E, Garcia-Molinero V and Rodriguez-Navarro S (2012) mRNA export and gene expression: the SAGA-TREX-2 connection. *Biochim. Biophys. Acta* **1819:** 555–565

Garcia-Pichardo D, Cañas JC, Garcia-Rubio ML, Gómez-González B, Rondón AG and Aguilera A (2017) Histone Mutants Separate R Loop Formation from Genome Instability Induction. *Mol. Cell* **66:** 597-609.

Garcia-Rubio M, Aguilera P, Lafuente-Barquero J, Ruiz JF, Simon M-N, Géli V, Rondón AG and Aguilera A (2018) Yra1-bound RNA-DNA hybrids cause orientation-independent transcription-replication collisions and telomere instability. *Genes Dev.* **32:** 965–977

Gavaldá S, Santos-Pereira JM, Garcia-Rubio ML, Luna R and Aguilera A (2016) Excess of Yra1 RNA-Binding Factor Causes Transcription-Dependent Genome Instability, Replication Impairment and Telomere Shortening. *PLoS Genet.* **12:** e1005966

Gómez-González B and Aguilera A (2019) Transcription-mediated replication hindrance: a major driver of genome instability. *Genes Dev.***:** 1–19

Gómez-Saldivar G, Fernandez A, Hirano Y, Mauro M, Lai A, Ayuso C, Haraguchi T, Hiraoka Y, Piano F, Askjaer P (2016) Identification of Conserved MEL-28/ELYS Domains with Essential Roles in Nuclear Assembly and Chromosome Segregation. PLoS Genet.**12**: e1006131.

González-Aguilera C, Tous C, Gómez-González B, Huertas P, Luna R and Aguilera A (2008) The THP1-SAC3-SUS1-CDC31 complex works in transcription elongation-mRNA export preventing RNA-mediated genome instability. *Mol. Biol. Cell* **19:** 4310–4318

Gowrishankar J and Harinarayanan R (2004) Why is transcription coupled to translation in bacteria? *Mol. Microbiol.* **54:** 598–603

Groh M, Lufino MMP, Wade-Martins R and Gromak N (2014) R-loops associated with triplet repeat expansions promote gene silencing in Friedreich ataxia and fragile X syndrome. *PLoS Genet.* **10:** e1004318

Hamperl S, Bocek MJ, Saldivar JC, Swigut T and Cimprich KA (2017) Transcription-Replication Conflict Orientation Modulates R-Loop Levels and Activates Distinct DNA Damage Responses. *Cell* **170:** 774-786.e19

Huertas P and Aguilera A (2003) Cotranscriptionally formed DNA:RNA hybrids mediate transcription elongation impairment and transcription-associated recombination. *Mol. Cell* **12:** 711–721

Jani D, Lutz S, Hurt E, Laskey RA, Stewart M and Wickramasinghe VO (2012) Functional and structural characterization of the mammalian TREX-2 complex that links transcription with nuclear messenger RNA export. *Nucleic Acids Res.* **40:** 4562–4573

Jaramillo-Lambert A, Ellefson M, Villeneuve AM and Engebrecht J (2007) Differential timing of S phases, X chromosome replication, and meiotic prophase in the C. elegans germ line. *Dev. Biol.* **308:** 206–221

Krogan NJ, Lam MHY, Fillingham J, Keogh M-C, Gebbia M, Li J, Datta N, Cagney G, Buratowski S, Emili A and Greenblatt JF (2004) Proteasome involvement in the repair of DNA double-strand breaks. *Mol. Cell* **16:** 1027–1034

Lang KS, Hall AN, Merrikh CN, Ragheb M, Tabakh H, Pollock AJ, Woodward JJ, Dreifus JE and Merrikh H (2017) Replication-Transcription Conflicts Generate R-Loops that Orchestrate Bacterial Stress Survival and Pathogenesis. *Cell* **170:** 787-799.e18

Lei EP, Stern CA, Fahrenkrog B, Krebber H, Moy TI, Aebi U and Silver PA (2003) Sac3 is an mRNA export factor that localizes to cytoplasmic fibrils of nuclear pore complex. *Mol. Biol. Cell* **14:** 836–847

Lee SJ, Gartner A, Hyun M, Ahn B and Koo HS (2010) The Caenorhabditis elegans Werner syndrome protein functions upstream of ATR and ATM in response to DNA replication inhibition and double-strand DNA breaks. *PLoS Genet.* **6**:e1000801.

Li X and Manley JL (2005) Inactivation of the SR protein splicing factor ASF/SF2 results in genomic instability. *Cell* **122:** 365–378

Loomis EW, Sanz LA, Chédin F and Hagerman PJ (2014) Transcription-associated R-loop formation across the human FMR1 CGG-repeat region. *PLoS Genet.* **10:** e1004294

Luna R, Rondón AG and Aguilera A (2012) New clues to understand the role of THO and other functionally related factors in mRNP biogenesis. *Biochim. Biophys. Acta* **1819:** 514–520

M**arnef A and Legube G** (2020) R-loops as Janus-faced modulators of DNA repair. *Nat Cell Biol*. **23**: 305-313.

Marston NJ, Richards WJ, Hughes D, Bertwistle D, Marshall CJ and Ashworth A (1999) Interaction between the product of the breast cancer susceptibility gene BRCA2 and DSS1, a protein functionally conserved from yeast to mammals. *Mol. Cell. Biol.* **19:** 4633–4642

Martin JS, Winkelmann N, Petalcorin MIR, McIlwraith MJ and Boulton SJ (2005) RAD-51-dependent and -independent roles of a Caenorhabditis elegans BRCA2-related protein during DNA double-strand break repair. *Mol. Cell. Biol.* **25:** 3127–3139

Owen-Hughes T and Gkikopoulos T (2012) Making sense of transcribing chromatin. *Curr. Opin. Cell Biol.* **24:** 296–304

Pispa J, Palmén S, Holmberg CI and Jäntti J (2008) C. elegans dss-1 is functionally conserved and required for oogenesis and larval growth. *BMC Dev. Biol.* **8:** 51

Ródenas E, González-Aguilera C, Ayuso C and Askjaer P (2012) Dissection of the NUP107 nuclear pore subcomplex reveals a novel interaction with spindle assembly checkpoint protein MAD1 in Caenorhabditis elegans. *Mol. Biol. Cell* **23:** 930–944

Rondón AG, Jimeno S and Aguilera A (2010) The interface between transcription and mRNP export: from THO to THSC/TREX-2. *Biochim. Biophys. Acta* **1799:** 533–538

Santos-Pereira JM, Garcia-Rubio ML, González-Aguilera C, Luna R and Aguilera A (2014) A genome-wide function of THSC/TREX-2 at active genes prevents transcription-replication collisions. *Nucleic Acids Res.* **42:** 12000–12014

Skourti-Stathaki K, Kamieniarz-Gdula K and Proudfoot NJ (2014) R-loops induce repressive chromatin marks over mammalian gene terminators. *Nature* **516:** 436–439

Stergiou L, Eberhard R, Doukoumetzidis K, Hengartner MO (2011) NER and HR pathways act sequentially to promote UV-C-induced germ cell apoptosis in Caenorhabditis elegans. *Cell Death Differ*. **18**: 897-906.

Umlauf D, Bonnet J, Waharte F, Fournier M, Stierle M, Fischer B, Brino L, Devys D and Tora L (2013) The human TREX-2 complex is stably associated with the nuclear pore basket. *J. Cell Sci.* **126:** 2656–2667

Wellinger RE, Prado F and Aguilera A. (2006) Replication fork progression is impaired by transcription in hyperrecombinant yeast cells lacking a functional THO complex. *Mol Cell Biol.* **26**: 3327-34.

West SC (2003) Molecular views of recombination proteins and their control. *Nat. Rev. Mol. Cell Biol.* **4:** 435–445

Wilmes GM, Bergkessel M, Bandyopadhyay S, Shales M, Braberg H, Cagney G, Collins SR, Whitworth GB, Kress TL, Weissman JS, et al. (2008) A genetic interaction map of RNA-processing factors reveals links between Sem1/Dss1-containing complexes and mRNA export and splicing. *Mol. Cell* **32:** 735–746

Yang H, Jeffrey PD, Miller J, Kinnucan E, Sun Y, Thoma NH, Zheng N, Chen PL, Lee WH and Pavletich NP (2002) BRCA2 function in DNA binding and recombination from a BRCA2-DSS1-ssDNA structure. *Science* **297:** 1837–1848

FIGURES

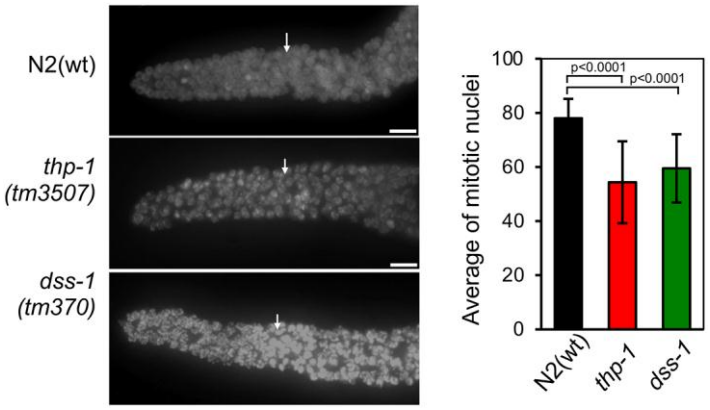

Figure 1. Mitosis characterization of THSC/TREX-2 *C. elegans* mutants.
Representative images of mitotic region of fixed germlines counterstained with DAPI from adult hermaphrodites of the indicated phenotypes. The arrow indicates the initiation of the transition zone. On the right, quantification of mitotic nuclei of N2(wt), *thp-1* and *dss-1* strains (n=8, n=15 and n=10, respectively). Error bars indicate standard deviation. Unpaired t-test two-tailed analysis. Scale bar 10µm.

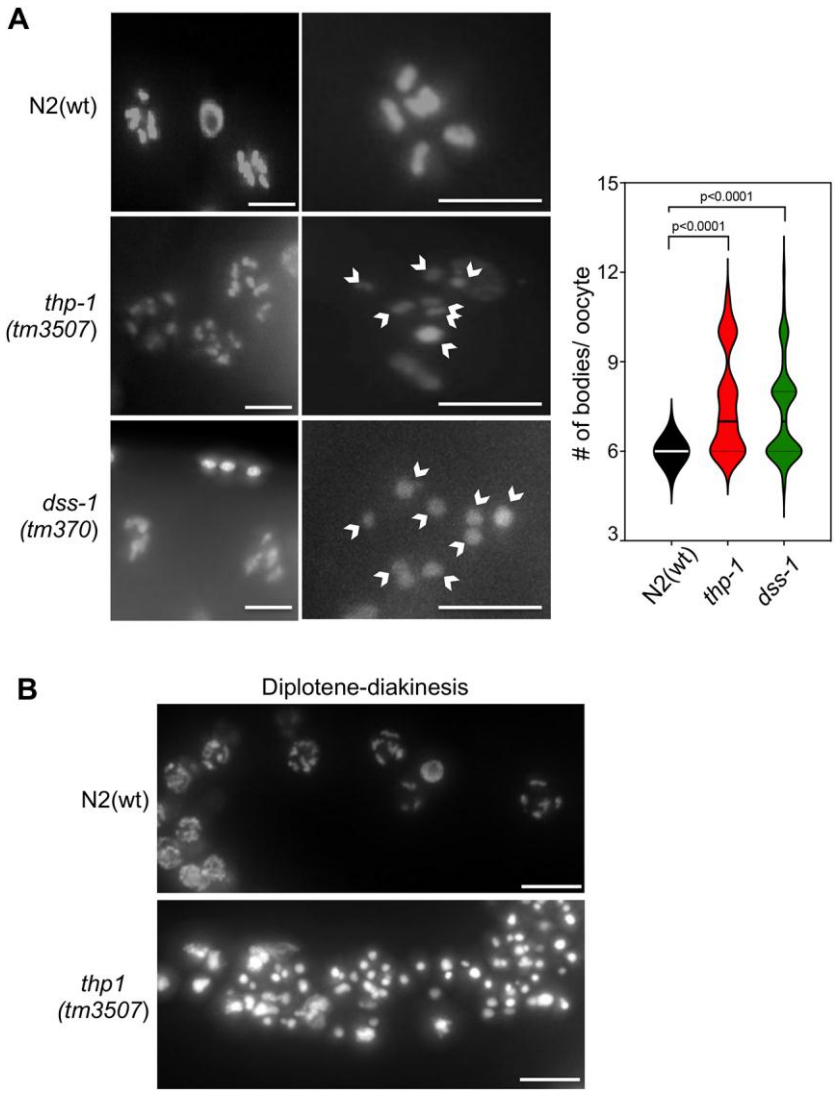

Figure 2. Diakinesis is abnormal in THSC/TREX-2 *C. elegans* mutants.

(A) Representative images of diakinesis germline region of fixed germlines counterstained with DAPI from wild-type N2 and *thp-1* adult hermaphrodites. Right shows the magnification of a single oocyte. On the right, quantification of DAPI-stained bodies in oocytes from N2(wt), *thp-1* and *dss-1* strains (n=51, n=45 and n=65, respectively). Error bars indicate standard deviation. Unpaired t-test two-tailed analysis. Scale bar 5µm.

(B) Representative images of diplotene/diakinesis region of fixed germlines from 36h post-L4 hermaphrodites of N2(wt) and thp-1(tm3507) strains. Scale bar 10µm.

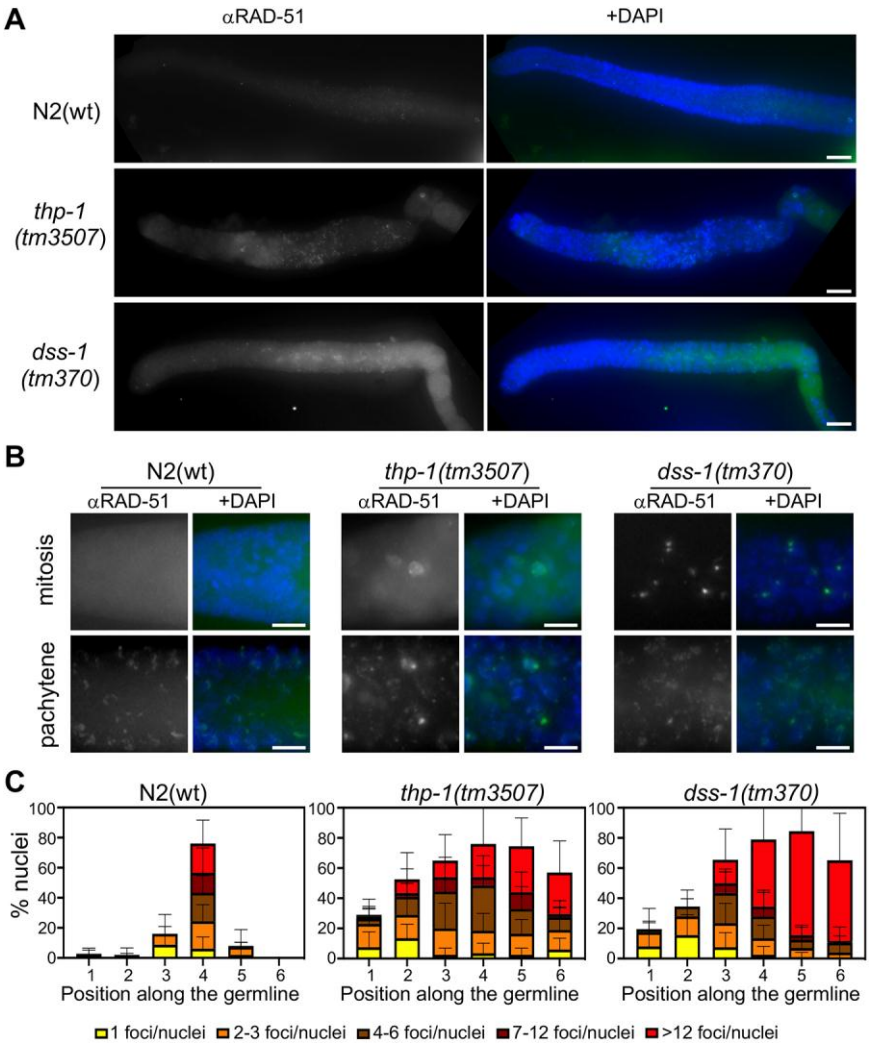

Figure 3. *C. elegans thp-1* and *dss-1* mutants show increased levels of RAD-51 foci.

(A) Representative images of completed fixed germlines of adult hermaphrodites from the indicated genotypes immunostained with anti-RAD-51 antibodies and counterstained with DAPI. Scale bar 10µm.

(B) Representative images of the mitotic and the pachytene regions of fixed germlines of adult hermaphrodites from the indicated genotypes immunostained with anti-RAD-51 antibodies and counterstained with DAPI. Scale bar 5µm.

(C) Quantification of RAD-51 foci of germline nuclei. Zone 1 (mitosis), zone 2 (transition zone), zones 3-4-5 (pachytene), zone 6 (diplotene) of N2(wt), *thp-1* and *dss-1* strains (n=18, n=20 and n=20, respectively). Error bars indicate standard deviation. Statistical analysis is shown in figure S3.

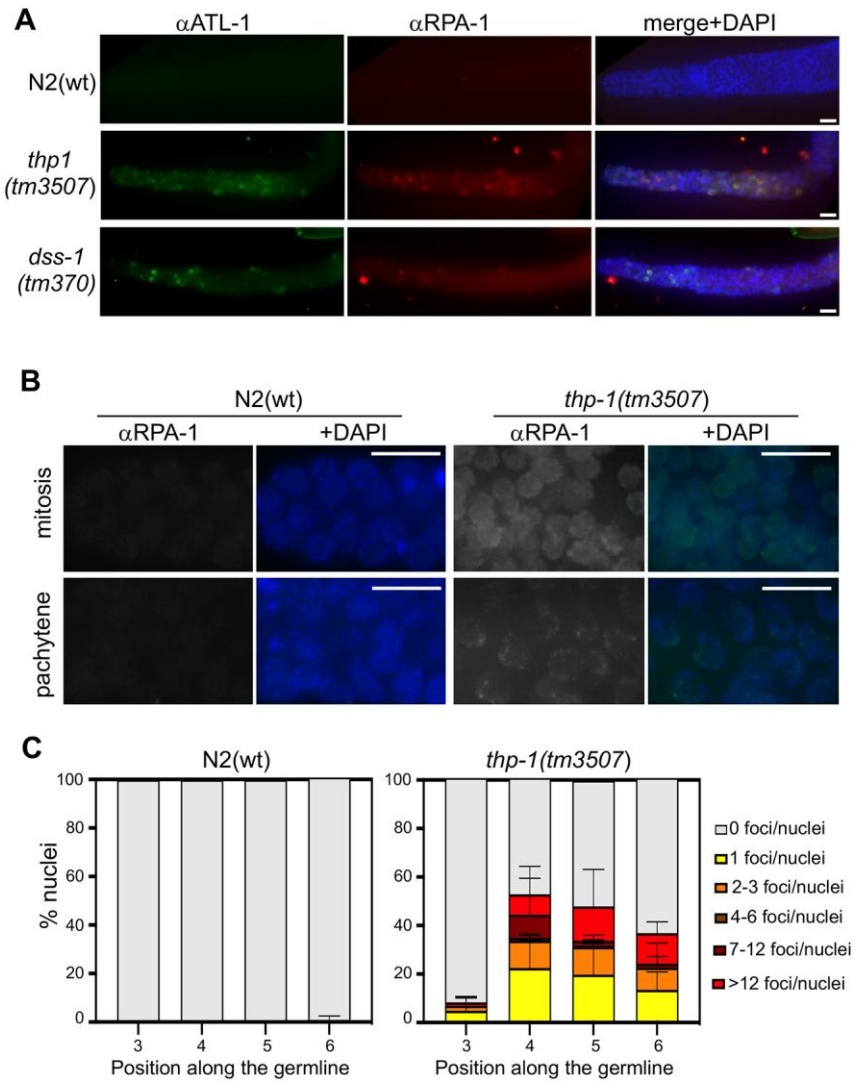

Figure 4. THSC/TREX-2 mutants show DNA damage accumulation and checkpoint activation.

A) Representative images of fixed germlines of adult hermaphrodites immunostained with anti-ATL-1 and anti-RPA-1 antibodies and counterstained with DAPI from animals of the indicated genotypes. Scale bar 10µm.

(B) Representative images of fixed germlines of adult hermaphrodites immunostained for RPA-1::YFP and counterstained with DAPI from animals N2(wt) and *thp-1* carrying the rpa-1::yfp. Scale bar 5µm.

(C) Quantification of RPA-1::YFP foci of all germline nuclei. Zone 3-4-5-6 equal parts of the pachytene region of animals as in (B) (n=3 each). Error bars indicate standard deviation. Statistical analysis is shown in Figure S4.

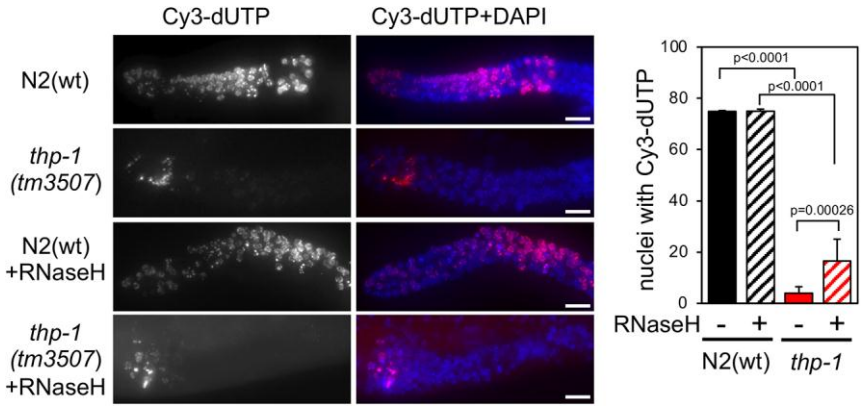

Figure 5. Mitotic replication is impaired in *C. elegans thp-1* germlines and partially alleviated by RNase H microinjection.

Representative images of fixed germlines of indicated genotype of adult hermaphrodites 2.5 hours after microinjection with Cy3-dUTP +/- RNase H. Graph shows the average of mitotic nuclei with Cy3-dUTP incorporation of N2(wt) and *thp-1* each untreated or treated with RNaseH (n=19, n=15, n=25 and n=15, respectively). Error bars indicate standard deviation. Unpaired t-test two-tailed analysis. Scale bar 10µm.

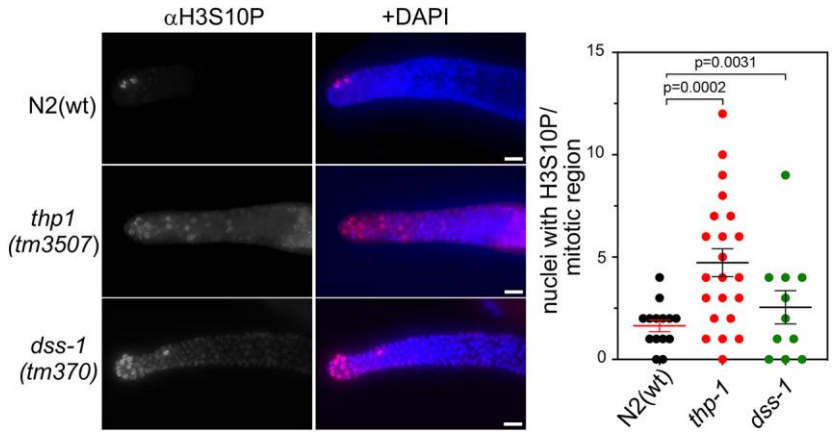

Figure 6. THSC/TREX-2 mutants show mild H3S10P accumulation.
Representative images of fixed germlines of adult hermaphrodites immunostained with anti-H3S10P antibody and counterstained with DAPI from the indicated genotypes. Graph shows the number of mitotic nuclei with H3S10P signal per gonad of the N2(wt), *thp-1* and *dss-1* strains (n=14, n=22 and n=11, respectively). Mean and standard deviation are shown. Two-tailed unpaired T- test. Scale bar 10µm.

Table 1. *C. elegans thp-1* is an essential gene.

Genotype	n	Total eggs	Viable progeny	Percent lethality	Brood size[b]
N2 (wt)	7	1998	1997	0.05	285.4±20.4
thp-1(tm3507) heterozygous	11	2188	725	62.86[c]	218.8±37.3
thp-1(tm3507) homozygous[a]	6	0	0	NA	

Embryonic lethality was scored by comparing the number of eggs that hatch to produce viable progeny versus the total number of eggs laid. [a] Hermaphrodites used were homozygous thp-1 mutants derived from thp-1 -/+ parents. [b]Average brood size ± SD ($p<0.001$; Student's t-Test). [c]The expected lethality for carrying the hT2 balancer chromosomes is 68.75%.

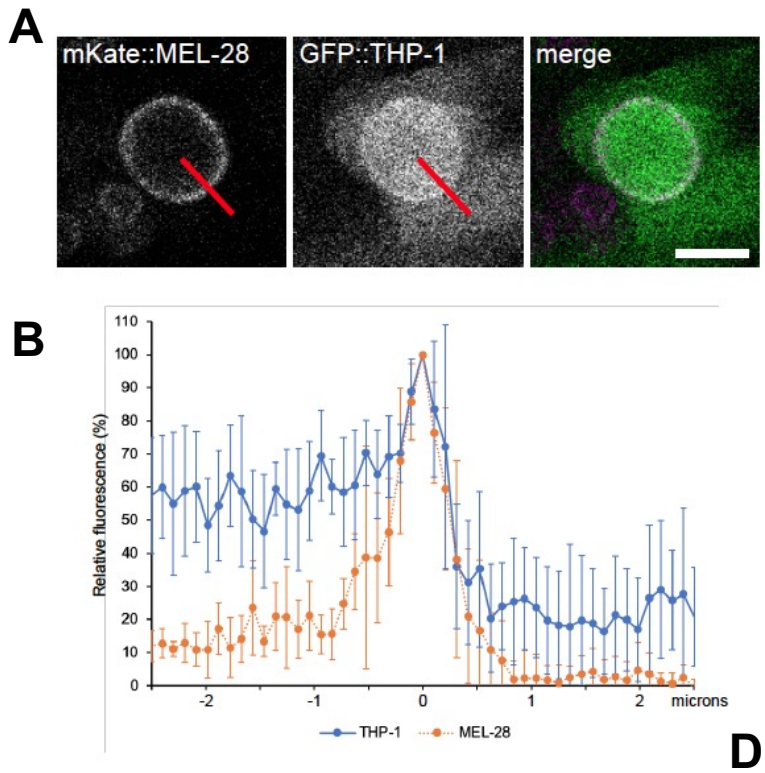

Fig. S1. Characterization of *C. elegans thp-1* (C27F2.10).
(A) Micrographs of a cell expressing mKate2::MEL-28 (magenta in merge) and GFP::THP-1 (green in merge). Fluorescence signal intensities were quantified along the red lines, background subtracted and normalized to the point with highest intensity. Scale bar 5 µm. (B) Average fluorescent intensities from five cells. Negative and positive values on the x-axis refer to signal in the nucleoplasm and the cytoplasm, respectively, whereas values close to zero on the x-axis correspond to the nuclear envelope. Note that both, mKate2::MEL-28 and GFP::THP-1 accumulate at the nuclear envelope. Error bars indicate standard deviation. (C) Scheme of *thp-1* gene structure and the predicted protein product for wild-type N2 and *thp-1(tm3507)* deletion allele. *thp-1(tm3507)* carries a 253 bp deletion in exon 4 that generates a premature stop codon. (D) Nested single worm *thp-1(tm3507)* PCR with *thp-1* specific primers for *tm3507* deletion. Wild-type N2 (lane 3) and *thp-1* (lane 2) showing the 253 bp deletion.

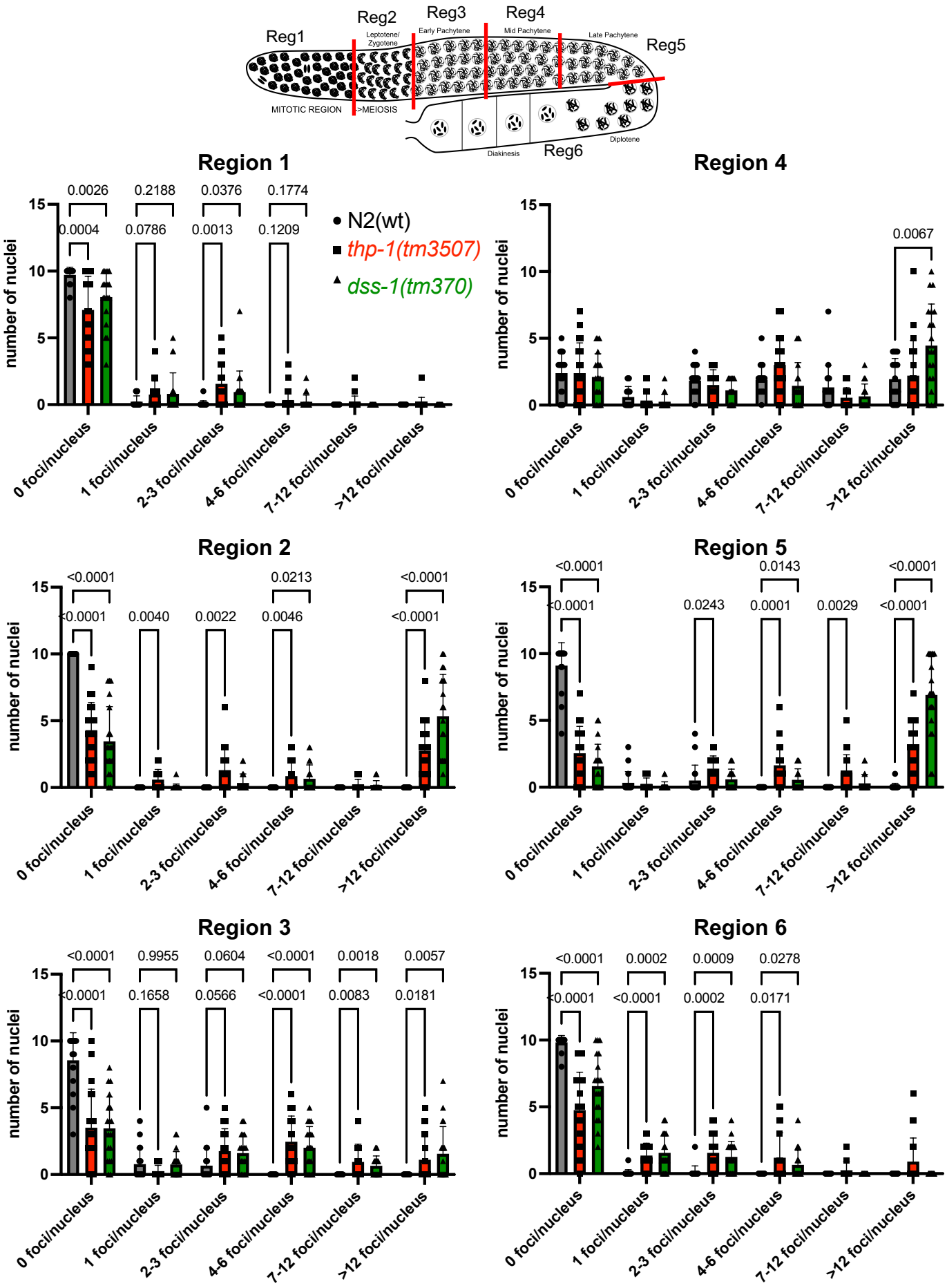

Fig. S2. RAD-51 accumulation in *C. elegans thp-1* and dss-1 mutants.
Scheme indicating the gonad regions. Graphs show the quantification of RAD-51 foci of germline nuclei. Zone 1 (mitosis), zone 2-3-4-5 equal parts of the meiotic region from transition zone to late pachytene from N2(wt) and *thp-1* strains (n=18, n=10 and n=20, respectively). Error bars indicate standard deviation. 2way ANOVA test.

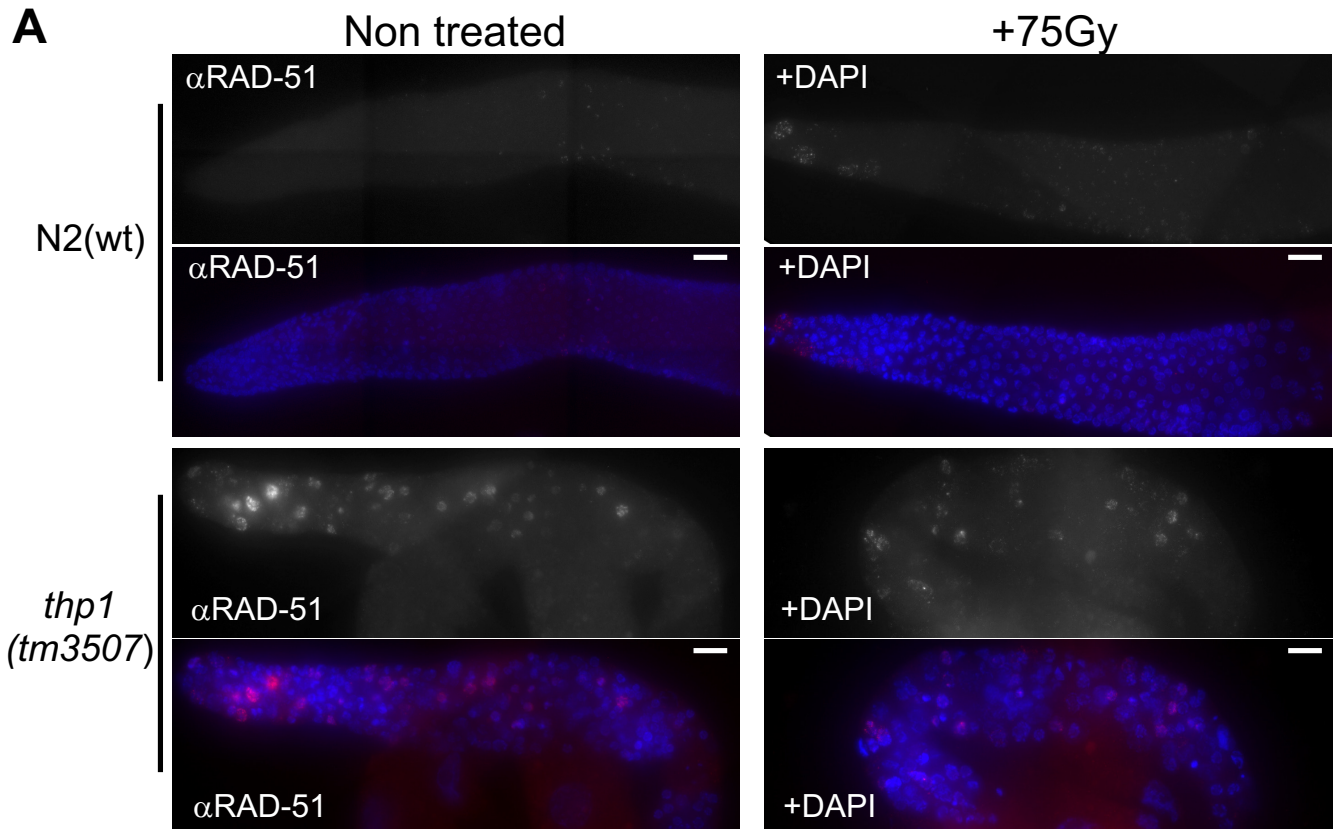

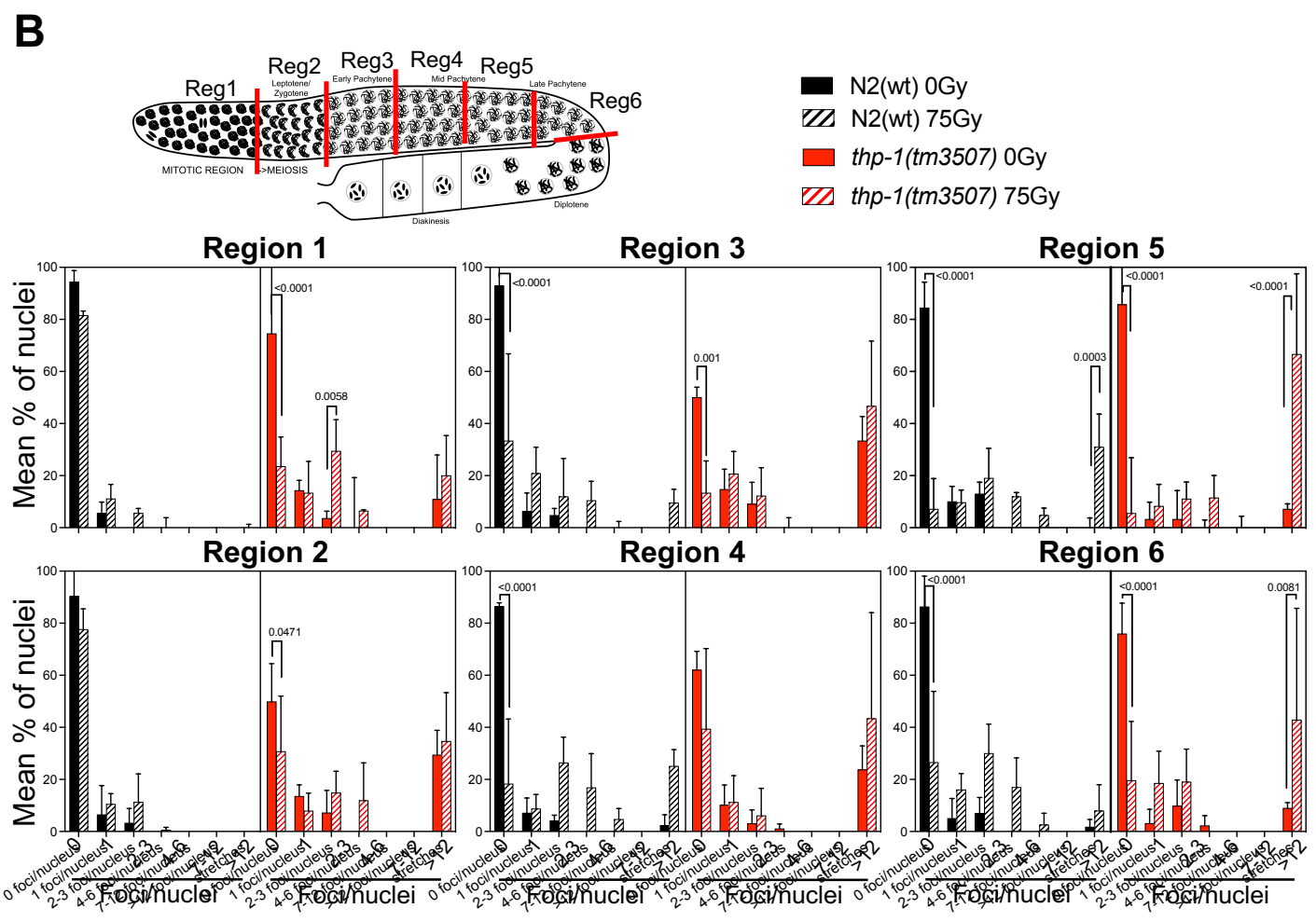

Figure S3. *C. elegans thp-1* mutant show a delay in DSB repair.
(A) Representative images of fixed germlines of indicated genotype of 48-72 post-L4 hermaphrodites, with or without 75Gy irradiation, immunostained with anti-RAD-51 antibodies and counterstained with DAPI. Scale bar 10μm.
(B) Scheme indicating the gonad regions. Graphs show the quantification of RAD-51 foci of germline nuclei. Zone 1 (mitosis), zone 2-3-4-5 equal parts of the meiotic region from transition zone to late pachytene from N2(wt) and *thp-1* strains (n=3 each). Error bars indicate standard deviation. 2way ANOVA test.

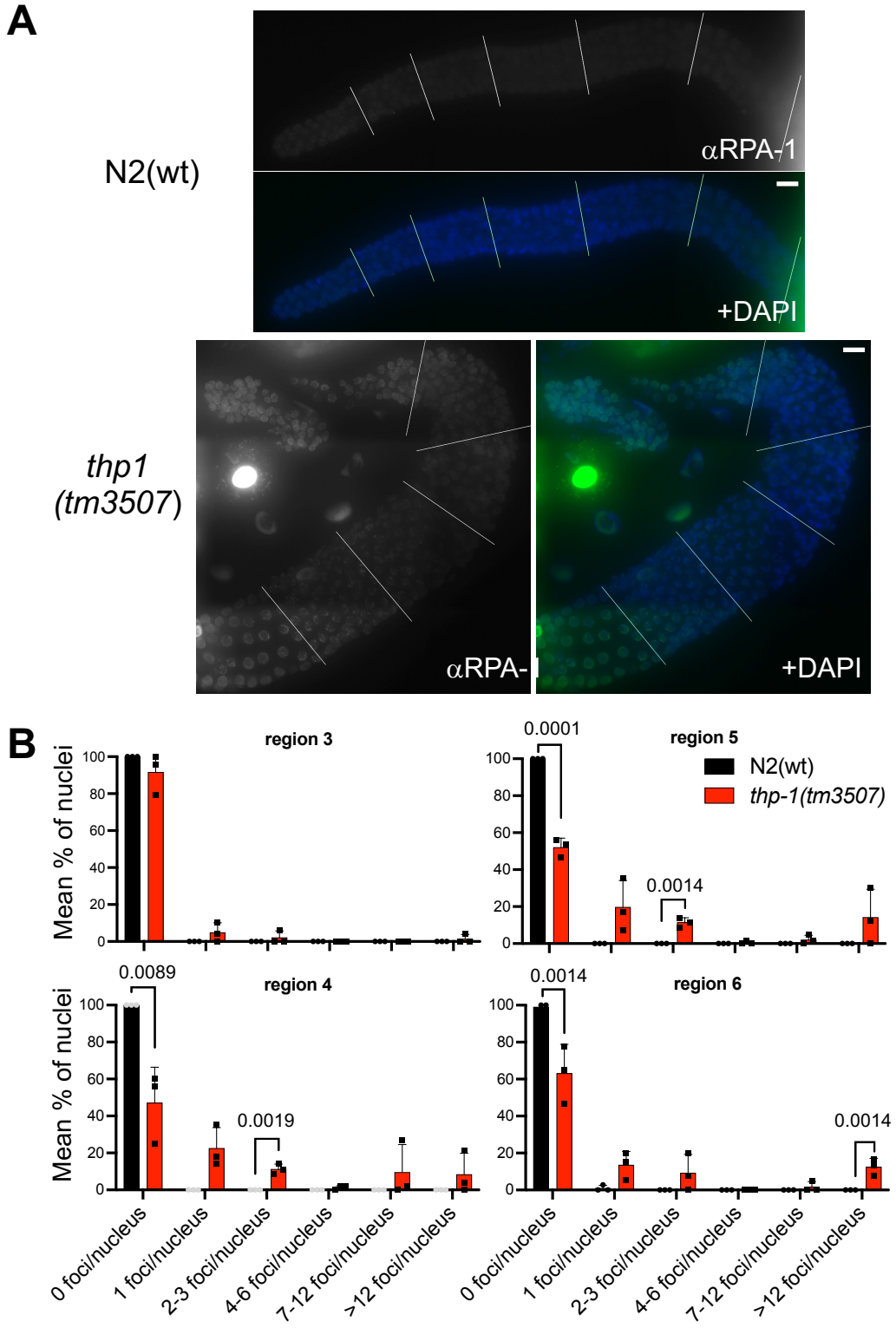

Fig. S4. *C. elegans thp-1* mutant show RPA-1 accumulation.
(A) Representative images of fixed germlines of N2(wt) and *thp-1*, carrying *rpa-1::yfp,* adult hermaphrodites immunostained against RPA-1::YFP and counterstained with DAPI. Scale bar 10μm.
(B) Graphs show the quantification of RPA-1::YFP foci of germline nuclei. Zone 3-4-5-6 equal parts of the pachytene region from strains as in (A) (n=3 each). Error bars indicate standard deviation. Unpaired t-test two-tailed analysis.

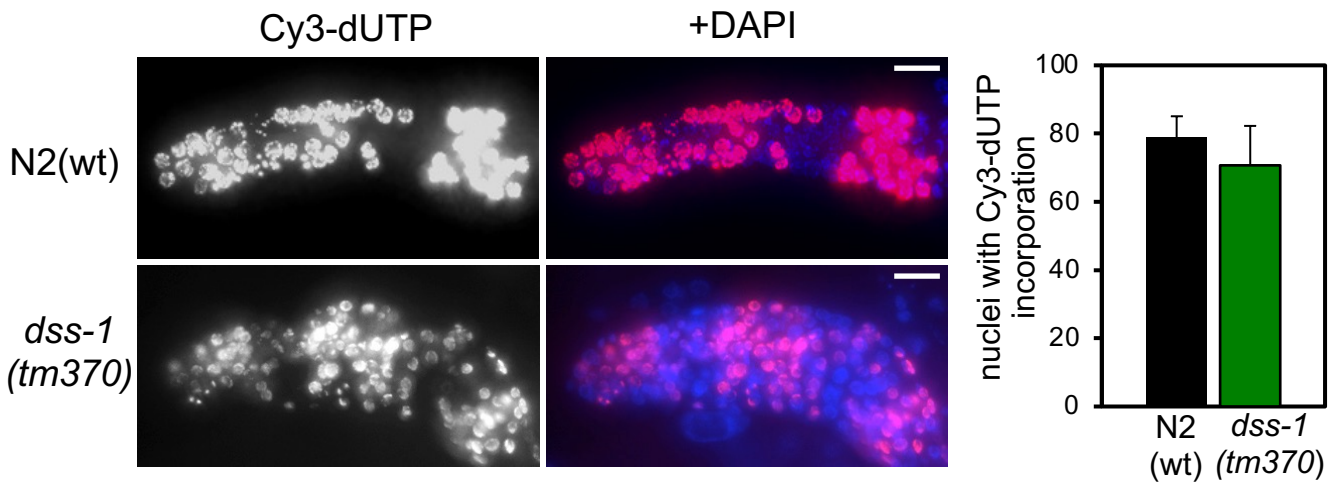

Fig. S5. Mitotic replication is normal in *C. elegans dss-1* germlines. Representative images of fixed germlines of indicated genotype of adult hermaphrodites 2.5 hours after microinjection with Cy3-dUTP. Graphs show the quantification of nuclei with Cy3-dUTP incorporation (n=3 each). Scale bar 10μm.

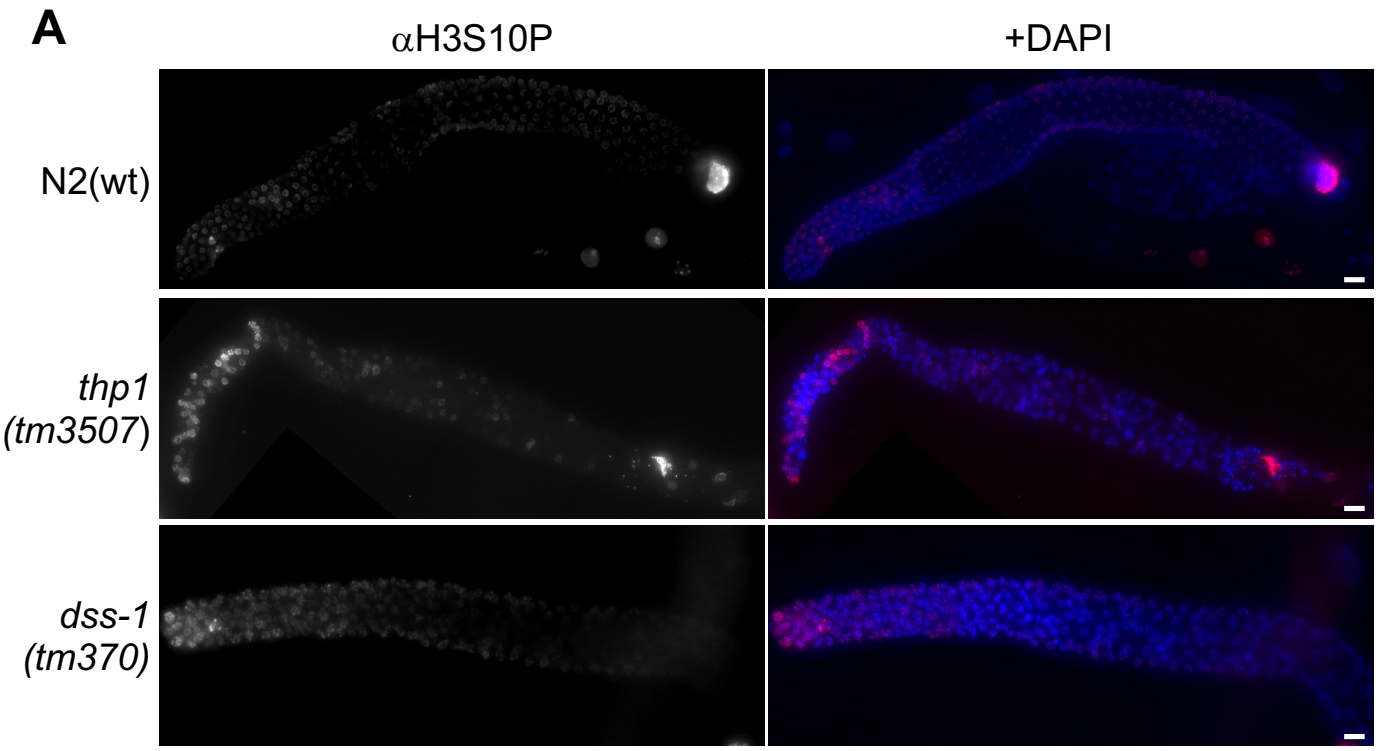

Fig. S6. THSC/TREX-2 mutants show mild H3S10P accumulation.
(A) Representative images of whole fixed germlines immunostained with anti-H3S10P antibody and counterstained with DAPI from N2(wt), *thp-1* and *dss-1* strains. Scale bar 10μm.
(B) Representative images of the diakinesis region immunostained with anti-H3S10P antibody and counterstained with DAPI from 36h post-L4 N2(wt), *thp-1* and *dss-1* strains. Scale bar 10μm.

Table S1. THSC/TREX-2 orthologs identify by bioinformatics search and blast similarity comparison with yeast and mammalian THSC/TREX-2 complex member.

C. elegans	*S. cerevisiae*			Mammalian		
Protein	Protein	BlastP e-value	% Identities	Protein	BlastP e-value	% Identities
C27F2.10	Thp1	2e-16	27	PCID2	e-118	45
DSS-1	Sem1	2e-11	40	DSS1	2e-13	49
T01C3.2	Sus1	0.045	20	ENY2	2.2	24
F20D12.2	Sac3	6e-26	28	GANP	7e-73	34
ND	Cdc13			Centrins		

ND. Not determined

Table S2. Primers

Name	Gene	Sequence 5'-3'
thp-1(tm3507)-E1	*thp-1*	ATTTAGCGCGCGCAGGACAA
thp-1(tm3507)-E2	*thp-1*	GAACGTGATCATTCGCAGCT
thp-1(tm3507)-I1	*thp-1*	CGACTTACGATGAGCACGCA
thp-1(tm3507)-I2	*thp-1*	GGGATGTTGGCATGTGACCA
dss-1(tm370)-E1	*dss-1*	TGAGGAATTTCCGGTTCAG
dss-1(tm370)-E2	*dss-1*	GTGGGGTACTGTAGCACCGC
dss-1(tm370)-I1	*dss-1*	GAAAAATCGGAATTTTTGGC
dss-1(tm370)-I2	*dss-1*	TGTGTGTGTAGGAATTGCGC

Table S3. *Antibodies*.

Antibody	Use	Source
Rabbit polyclonal αATL-1	IF(1:500)	Garcia-Muse and Boulton, 2005
Rabbit α-RAD-51	IF (1:800)	Alpi et al., 2003
Rabbit α-RAD-51	IF (1:10.000)	Novus #NB100-148
Rabbit α-RPA-1	IF(1:200)	Lee at el, 2010
Rabbit α-H3S10ph	IF(1:5000)	Millipore # 06-570
Mouse α-GFP	IF(1/500)	Roche #11814460001
AlexaFluor α-Rabbit::568	IF(1/500)	Life Tecnologies #A11011
AlexaFluor α-Rabbit::488	IF(1/5000)	Life Tecnologies #A11011
AlexaFluor α-Mouse::488	IF(1/500)	Life Tecnologies #A21200
AlexaFluor α-RAT::594	IF(1/500)	Life Tecnologies #A11007